ELSEVIER

Coordination Chemistry Reviews
190–192 (1999) 737–769

COORDINATION CHEMISTRY REVIEWS

www.elsevier.com/locate/ccr

Organic/inorganic composite materials: the roles of organoamine ligands in the design of inorganic solids

Douglas J. Chesnut [a], Douglas Hagrman [a], Pamela J. Zapf [a], Robert P. Hammond [a], Robert LaDuca Jr. [c], Robert C. Haushalter [b], Jon Zubieta [a,*]

[a] *Department of Chemistry, Syracuse University, Syracuse, NY 13244, USA*
[b] *Symyx Technologies, 3100 Central Expressway, Santa Clara, CA 95051, USA*
[c] *Department of Chemistry and Physics, Kings College, Wilkes-Barre, PA 18711, USA*

Accepted 6 April 1999

Contents

Abstract

The influence of organic components on the microstructure of inorganic solids has been extensively documented in recent years and has been shown to provide an efficacious method

* Corresponding author. Tel.: +1-315-443-2547; fax: +1-315-443-4070.
E-mail address: jazubiet@syr.edu (J. Zubieta)

PII: S0010-8545(99)00075-2

for the design of new materials. The synergism between the various chemical constituents at the organic/inorganic interface may result in imprinting of structural information from the organic molecules onto the inorganic framework. In this paper, the structural consequences of introducing organic components into several families of materials, including oxometalphosphates, transition metal oxides and transition metal halides and pseudohalides are briefly reviewed.

Keywords: Composite materials; Metal oxides; Organic templates; Metal halides

1. Introduction

The contemporary interest in solid state inorganic materials reflects their properties, which endow these materials with applications ranging from heavy construction to microcircuitry [1]. A powerful synthetic approach for the manipulation of the microstructures of solid state inorganic materials exploits the incorporation of organic components, which contribute to the increased complexity as one constituent in a hierarchical structure exhibiting a synergistic interaction between the organic and inorganic substructures [2,3]. Three primary classes of materials in which organic components play an important structural role have been studied extensively: zeolites [4], mesoporous oxides of the MCM-41 type [5], and biomineralized materials [6]. More recently, we have expanded the organic/inorganic oxide materials to include two new families: the microporous transition metal phosphates with entrained organic cations (TMPO's) [7–9] and the organically templated vanadium and molybdenum oxides [10–17]. This concept of templating anionic inorganic networks with organic constituents has also been extended by us to the metal halide and pseudohalide systems [18] in a demonstration of the wide-ranging applications of the general strategy.

2. The synthetic approach

2.1. Hydrothermal synthesis

The synthesis of these organically templated inorganic solids is not complicated to execute, but the large number of interacting variables renders the observation of many trends difficult. In the case of many inorganic materials, the synthesis must be performed at high temperatures (800–1200°C) because the starting materials are solid state compounds and the high temperatures are mandatory in order to achieve diffusion rates adequate for product formation within a reasonable time period. However, implicit in the evolution of organic–inorganic hybrid materials is a shift from the thermodynamic to the kinetic domain, so as to replace thermodynamic phases by structurally more complex metastable phases. Traditional high tempera-

ture solid state syntheses produce dense phases in which the structural integrity of the starting materials is often lost. Consequently, low temperature techniques similar to those used for small molecule chemistry must be adopted. Hydrothermal synthesis has been found to provide a powerful method for the preparation of organic–inorganic hybrid materials with retention of the structural elements of the reactants in the final products.

While well-established for the synthesis of zeolites, the hydrothermal method has more recently been adapted to the preparation of a wide variety of metastable materials, including TMPO's and even complex polyoxoalkoxometalates [18]. Hydrothermal reactions, typically carried out in the temperature range 120–260°C under autogenous pressure, exploit the self-assembly of the product from soluble precursors [19]. The reduced viscosity of water under these conditions enhances diffusion processes so that solvent extraction of solids and crystal growth from solution are favored [20]. Since differential solubility problems are minimized, a variety of simple precursors may be introduced, as well as a number of organic and/or inorganic structure-directing agents from which those of appropriate size and shape may be selected for efficient crystal packing during the crystallization process. Under such nonequilibrium crystallization conditions, metastable kinetic phases rather than the thermodynamic phase are most likely isolated [21]. While several pathways, including that resulting in the most stable phase, are available in such nonequilibrium mixtures, the kinetically favored structural evolution results from the smallest perturbations of atomic positions. Consequently, nucleation of a metastable phase may be favored. Thus, our general synthetic approach is to employ an organic component at low temperature to modify or control the surface of growing composite crystals in a hydrothermal medium.

2.2. The organic component

As shown in Fig. 1, the organic component of an organic–inorganic composite material may adopt a variety of roles depending on its structure, charge and presence of heterometallic sites: (i) as a charge-compensating, space filling and structure directing cation; (ii) as a ligand to a secondary transition metal center in

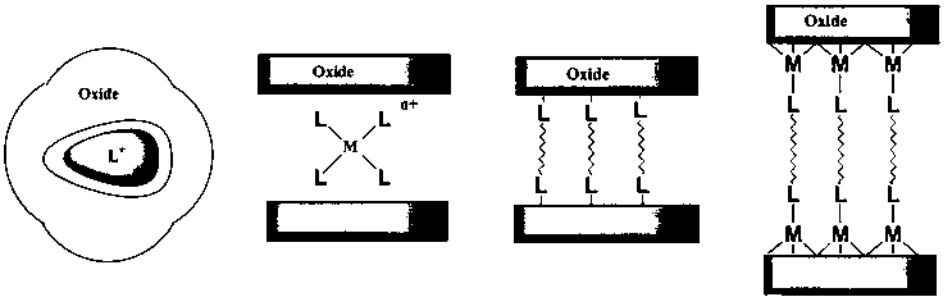

Fig. 1. A schematic representation of structural roles adopted by organonitrogen components of organic/inorganic composite solids.

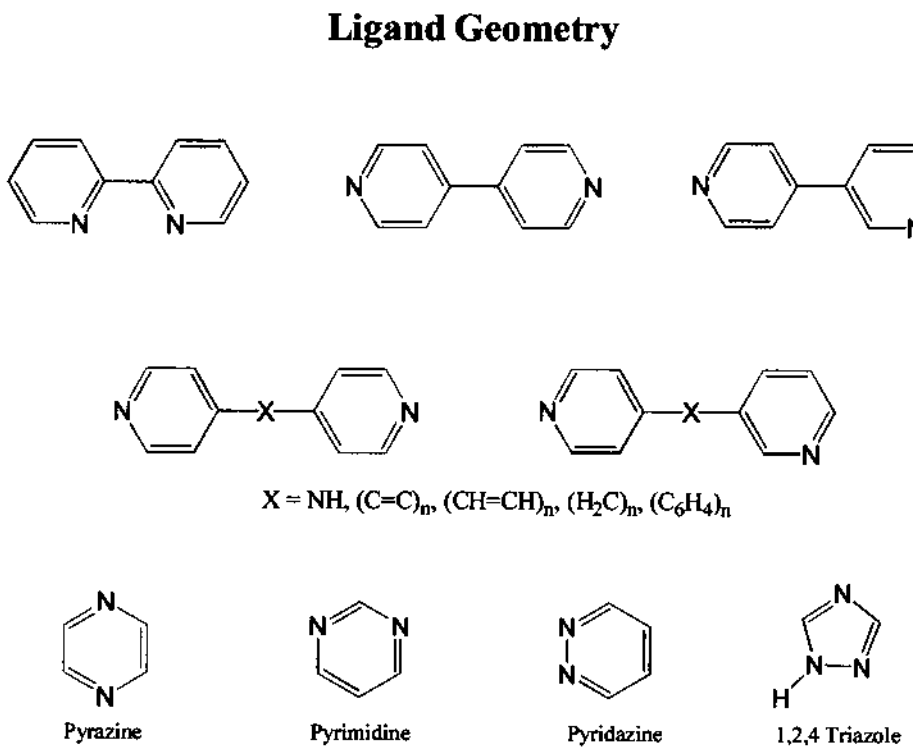

Fig. 2. Representative examples of organonitrogen ligand types.

a complex cation; and (iii) as a ligand bound directly to the inorganic matrix as a terminal group or as a pillar. In this latter case, the organic ligand may associate with the primary metal constituent of the inorganic substructure or with a secondary metal site of a heterobimetallic inorganic substructure. The present discussion will be limited to simple organonitrogen components, such as ethylenediamine, diaminobicyclooctane (DABCO) and the aromatic nitrogen donors of Fig. 2.

3. A representative oxovanadium phosphate framework

The structure directing role of organoamine cations in defining the architectures of composite oxides is dramatically illustrated by the structure of $[HN(CH_2CH_2)_3NH]K_{1.35}$ $[V_5O_9(PO_4)_2]\cdot x H_2O$ (VOPO-23) [9], shown in Fig. 3. This remarkable framework material is isolated in 95% yield from the hydrothermal reaction of KVO_3, DABCO and phosphoric acid at 200°C. The complex oxovanadium phosphate framework of VOPO-23 is constructed from the fundamental pentanuclear building block shown in Fig. 3b. The connectivity of these units results in extremely large voids in the framework which are occupied by twelve H_2DABCO^{2+}, 32 K^+, and about 64 H_2O molecules.

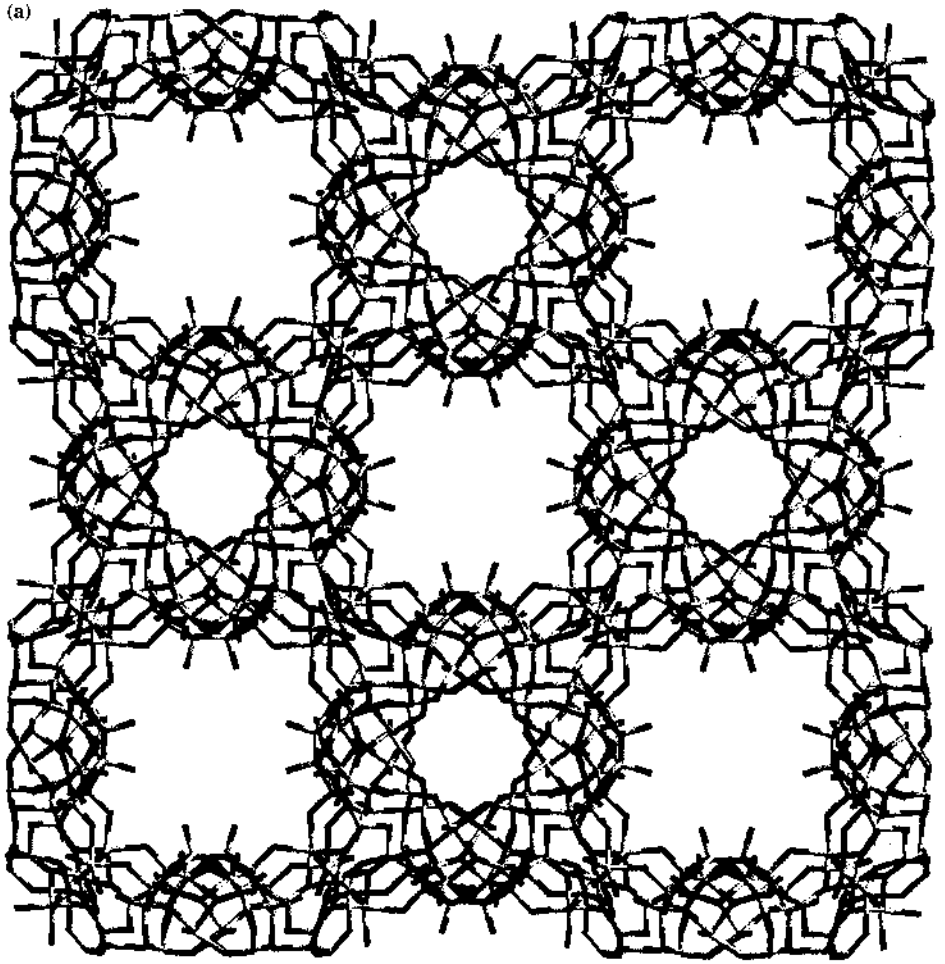

Fig. 3. (a) A view of the complex three-dimensional oxovanadium framework of $(H_2DABCO)K_{1.35}[V_5O_9(PO_4)_2]\cdot xH_2O$. (b) The pentanuclear fundamental building block of this oxovanadium phosphate framework.

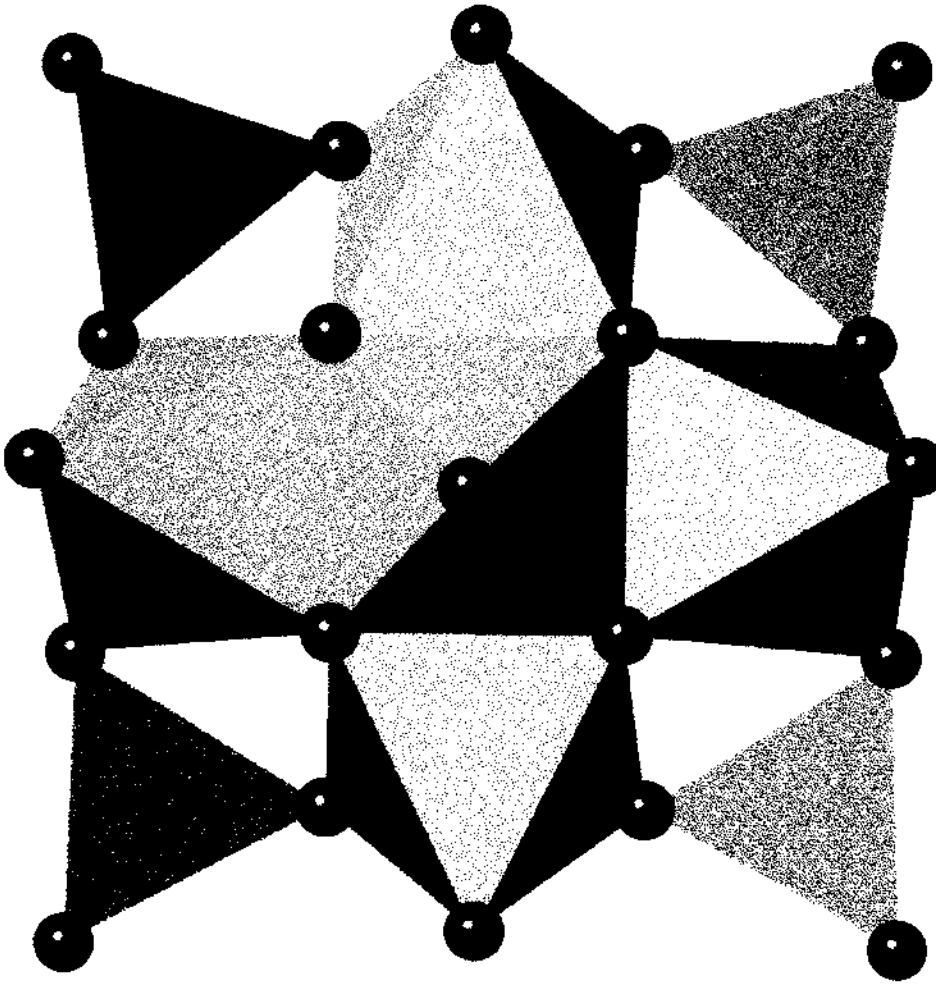

(b)

Fig. 3. (*Continued*)

The structure reveals two of the phenomena that critically influence the organization of the composite, namely hydrogen bonding and hydrophobic–hydrophilic interactions. The important structure directing role of the entrained organoammonium cation manifests itself in the strong, geometrically very specific hydrogen bonding between the N–H groups of the cation and O or O–H groups of the framework. The role of hydrophobic–hydrophilic interactions is likewise evident in the complex pattern of cation and water molecule occupancy of the cavities and the association of the {V=O} groups with the nonpolar organic cations.

4. The vanadium oxide lamellar structures

While organoammonium cations have been extensively exploited in the design of zeolites and of open-framework transition metal phosphates (TMPO's), it is also apparent that the structure directing role of the organoamine component may be introduced in the form of a coordination complex cation $\{M(H_2N\text{-linker-}NH_2)_x\}^{n+}$, which combines the space-filling, charge-compensating and potential multipoint hydrogen bonding associated with the organoammonium cation with the geometric constraints, stability and additional coordination potential of a transition metal complex cation. The introduction of cationic interlayer transition or post-transition metal complexes has allowed the preparation of a new class of layered, often mixed-valence vanadium oxides, whose structures are illustrated in Fig. 4.

The structures of $[\{Cu(en)_2\}V_6O_{14}]$ (VOXI-1) and $[\{Cu(en)_2\}_2V_{10}O_{25}]$ (VOXI-2) illustrate the common features of multipoint hydrogen bonding between the amine –NH protons and the network oxides and of partitioning of the structure into inorganic and organic domains. The materials also reveal the profound influence of minor modifications in reaction conditions on the detailed structures of the vanadium oxide layers. Thus, the layer of VOXI-1 contains infinite zig–zag chains of edge-sharing $\{VO_5\}$ square pyramids linked by $\{VO_4\}$ tetrahedra, with a V(V):V(IV) ratio of 1:2. In contrast, the structure of VOXI-2 consists of double strands of corner-sharing chains of trimeric edge-sharing $\{VO_5\}$ square pyramids linked by $\{VO_4\}$ tetrahedra, with a V(V):V(IV) ratio of 3:2.

The cationic components may, of course, be constructed from a variety of transition metal cations and organoamine ligands. An obvious expedient is to introduce as the organic component an amine incapable of effective hydrogen bonding to the oxide network, such as 2,2′-bipyridine. The resulting structures $[\{Cu(bpy)\}_2V_{12}O_{32}]$ (VOXI-3) and $[\{Cu(bpy)\}V_4O_{11}]$ (VOXI-4) exhibit a direct linkage of the coordination complex moiety $\{Cu(bpy)\}^{2+}$ to the oxo-groups of the vanadium oxide network to generate bimetallic oxide layers. In the case of VOXI-3, the network consists of V(V) oxide double sheets in which the Cu(II) centers occupy rectangular cavities in the $\{V_6O_6\}$ network. The Cu(II) sites adopt the common $4+2$ geometry associated with this d^9 metal. The bipyridyl ligands project into the interlamellar region in a parallel arrangement, maximizing π-stacking. The structure may be described in terms of inorganic layers alternating with organic domains, a common motif for layered organic/inorganic composites [22].

Once again, minor synthetic variations produce significant structural consequences as manifested in the structure of VOXI-4. While, in common with VOXI-3, the structure consists of vanadium oxide layers with $\{Cu(bpy)\}^{2+}$ units directly linked to the oxides of the layer and projecting bpy ligands, the network connectivity is quite distinct from that of VOXI-3. The layer consists of square pyramidal $\{VO_5\}$ sites edge sharing with $\{VO_4\}$ tetrahedra. The tetrahedral units form $\{CuV_4O_5\}$ rings with the square pyramidal Cu(II) sites in $4+1$ geometry, in contrast to the $4+2$ geometry observed for VOXI-3.

This family of materials of general formulation $[\{M(diamine)_z\}V_xO_y]$ should also allow structural modifications which reflect the coordination preferences of the divalent metal M. The structural influences of the amine-ligated site are evident in the structures of $[\{Zn(bpy)_2\}_2V_6O_{17}]$ (VOXI-5) and $[\{Zn(bpy)\}_2V_4O_{12}]$ (VOXI-6).

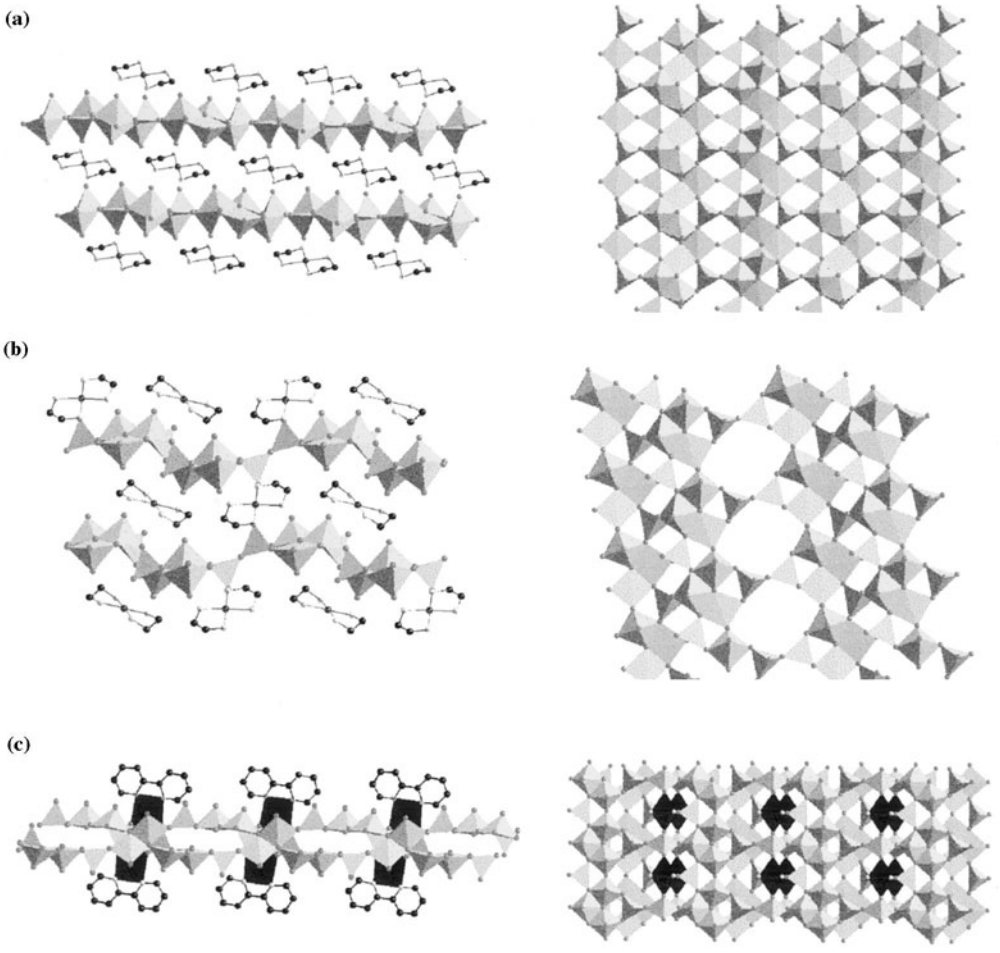

Fig. 4. Views parallel and perpendicular to the layers of (a) VOXI-1; (b) VOXI-2; (c) VOXI-3; (d) VOXI-4; (e) VOXI-5; and (f) VOXI-6.

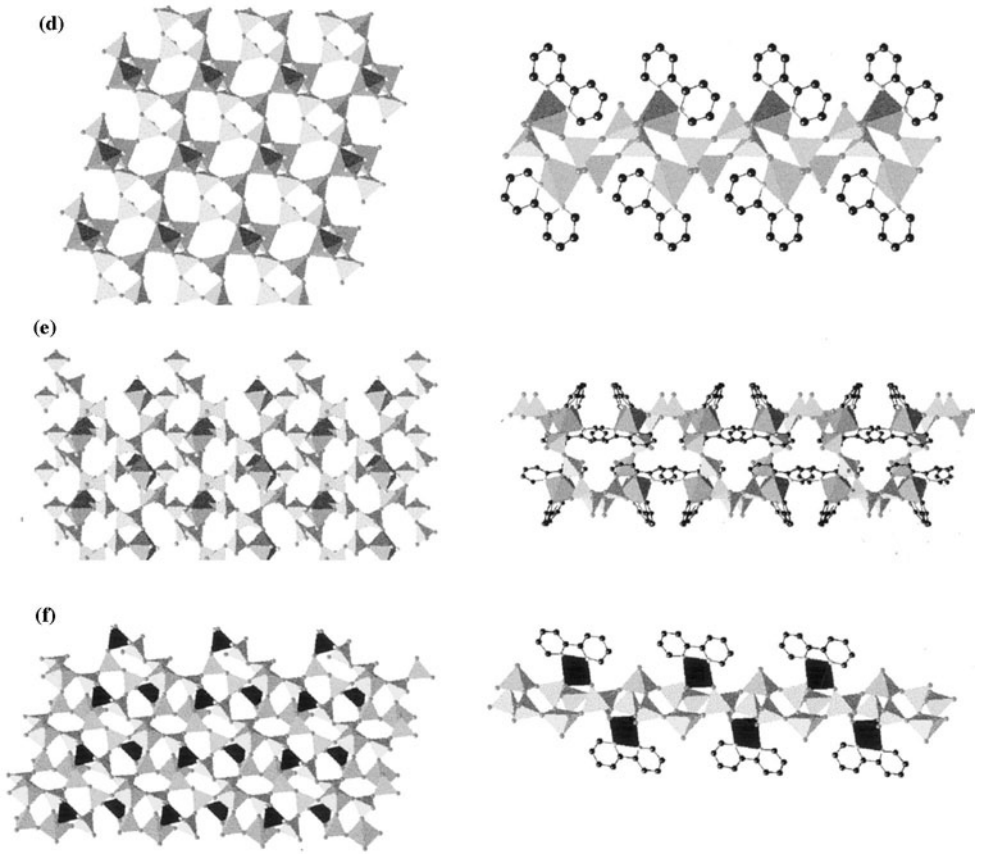

Fig. 4. (*Continued*)

The unprecedented structure of VOXI-5 consists of {VO} layers displaying a pronounced sinusoidal ruffling. The layers are composed of V(V) tetrahedra in a corner-sharing arrangement which generates large circular cavities defined by fourteen $\{VO_4\}$ tetrahedra and occupied by two $\{Zn(bpy)_2\}$ units. The bpy ligands protrude above and below the mean plane of the $\{V_{14}O_{14}\}$ ring to fill the troughs created by the ruffling of the layers.

In contrast, the structure of VOXI-6 is constructed from discrete $\{V_4O_{12}\}^{4-}$ clusters linked through $\{Zn(bpy)\}^{2+}$ square pyramids into a two dimensional network. While the $[V_4O_{12}]^{4-}$ molecular cluster is well-established [23], VOXI-6 represents a unique example of its occurrence as a substructure of a solid phase. In fact, minor modification of the reaction conditions yields the molecular cluster $[\{Zn(bpy)_2\}_2V_4O_{12}]$ [24]. It is also noteworthy that while the Zn(II) site of VOXI-5 exhibits $\{ZnN_4O_2\}$ geometry, the Zn(II) site of VOXI-6 is square pyramidal $\{ZnN_2O_3\}$ with coordination to a single bpy ligand.

5. Representative molybdenum oxide structure

The same strategies employed in the preparation of vanadium oxide-based composite materials may be applied to the molybdenum oxides. The methodology is illustrated by introducing $\{M(bpy)_n\}^{2+}$ subunits to modify the oxide structure, as demonstrated in the structures of $[\{Ni(bpy)\}_2Mo_4O_{13}]$ (MOXI-10), $[\{Cu(bpy)\}Mo_2O_7]$ (MOXI-17), and $[\{Co(bpy)\}Mo_3O_{10}]$ (MOXI-18), shown in Fig. 5.

The structure of MOXI-10 is constructed from β-$\{Mo_8O_{26}\}^{4-}$ clusters linked by $\{Ni(bpy)_2\}^{2+}$ bridges into a one-dimensional chain. It is instructive to note that the octamolybdate cluster in one of its five isomeric forms is a common substructure of phases of the {M(amine)}/Mo-oxide family, and is observed in $[\{Cu(en)_2\}_2Mo_8O_{26}]$ [25], $[\{Cu(4, 4'\text{-bpy})\}_4Mo_8O_{26}]$ [10], $[\{Cu(bpe)\}_4Mo_8O_{26}]$ [26], $[\{Ni(4, 4'\text{-bpy})_2(H_2O)_2\}_2Mo_8O_{26}]$ [10], and $[\{Cu_3(4,7\text{-phen})_3\}_2Mo_{14}O_{45}]$ [16].

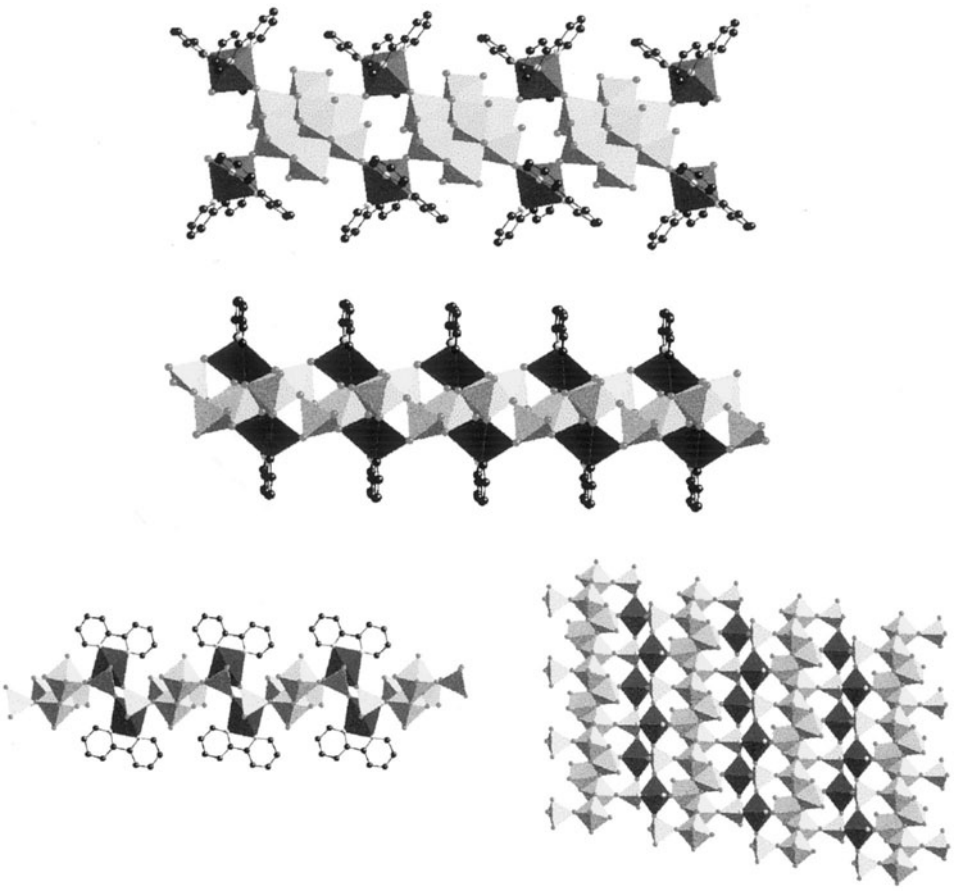

Fig. 5. Views of the structures of the molybdenum oxide phases (a) MOXI-10; (b) MOXI-17; and (c) MOXI-18 (parallel and perpendicular to the plane).

In contrast, the structure of MOXI-17 consists of a buckled one-dimensional molybdenum oxide chain linked to peripheral $\{CuN_2O_4\}$ octahedra. The $\{Mo_2O_7\}$ chain is constructed from edge-sharing $\{MoO_6\}$ octahedra and $\{MoO_5\}$ square pyramids. Each molybdenum octahedron shares common edges with a neighboring molybdenum octahedron, a molybdenum square pyramid, and two copper octahedra, and a common corner with one square-pyramidal unit. One square-pyramidal site engages in edge-sharing with an adjacent square pyramid and a molybdenum octahedron and displays corner-sharing with a second molybdenum octahedron and two $\{CuN_2O_4\}$ octahedra, while the second $\{MoO_5\}$ site exhibits edge-sharing to a square-pyramidal and an octahedral molybdenum site and corner-sharing to a $\{MoO_6\}$ site and a $\{CuN_2O_4\}$ octahedron. Consequently, each $\{CuN_2O_4\}$ unit links to four molybdenum polyhedra of the chain, sharing four vertices in two edge and two corner interactions with the molybdenum sites. The folding of the molybdenum chain reflects the incorporation of the $\{CuN_2O_4\}$ units through four-point, two-edge attachments and illustrates the role of the M^{2+} site in defining chain geometry.

Since one-dimensional molybdenum oxide chains are a recurring theme in oxide structural chemistry, the incorporation of appropriate metal–ligand subunits should allow bridging into higher dimensional solids. The structure of MOXI-18 illustrates this point. The structure consists of one-dimensional molybdenum oxide chains, constructed of molybdenum tetrahedra, octahedra and square pyramids, linked through $\{CoN_2O_4\}$ octahedra into a two-dimensional covalent network. The oxide chain itself results from the edge-sharing of $\{MoO_6\}$ octahedra and $\{MoO_5\}$ square pyramids. The $\{MoO_4\}$ tetrahedra link to the chain through a single corner-sharing interaction, but bridge two $\{CoN_2O_4\}$ octahedra through two additional corner-sharing linkages. Each Co site is defined by the nitrogen donors of the bpy ligand and four oxygen donors from three $\{MoO_4\}$ groups and one $\{MoO_6\}$ octahedron. The overall structure may be described as folded chains of edge-sharing molybdenum polyhedra linked through double chains of alternating $\{CoN_2O_4\}$ octahedra and $\{MoO_4\}$ tetrahedra into a two-dimensional network.

Not only may the coordination preference of the divalent metal–amine substructure influence the architecture of the oxide, but the ligand geometry may also be modified so as to introduce new constraints into the composite structure. One approach to the crystal engineering of coordination polymers has exploited appropriate metal centers that are linked through suitable polydentate ligands for the self-assembly of extended networks [27]. Polyfunctional rod-like ligands such as 4, 4′-bipyridine have been found to provide effective tethers for the construction of extended solids with various topologies [28]. This diversity of topologies adopted by metal-bridging organonitrogen solids and the variability of the channel dimensions associated with these structures suggested that metal oxide clusters or low-dimensional subunits could be incorporated into the void space in the $\{M(N\text{-linker-}N)_x\}^{n+}$ scaffolding. It was naively anticipated that the structure of the oxide component would conform to the constraints of the cationic skeleton, as illustrated schematically in Fig. 6 for one-, two- or three-dimensional complex cations providing anion vacancies of various dimensions.

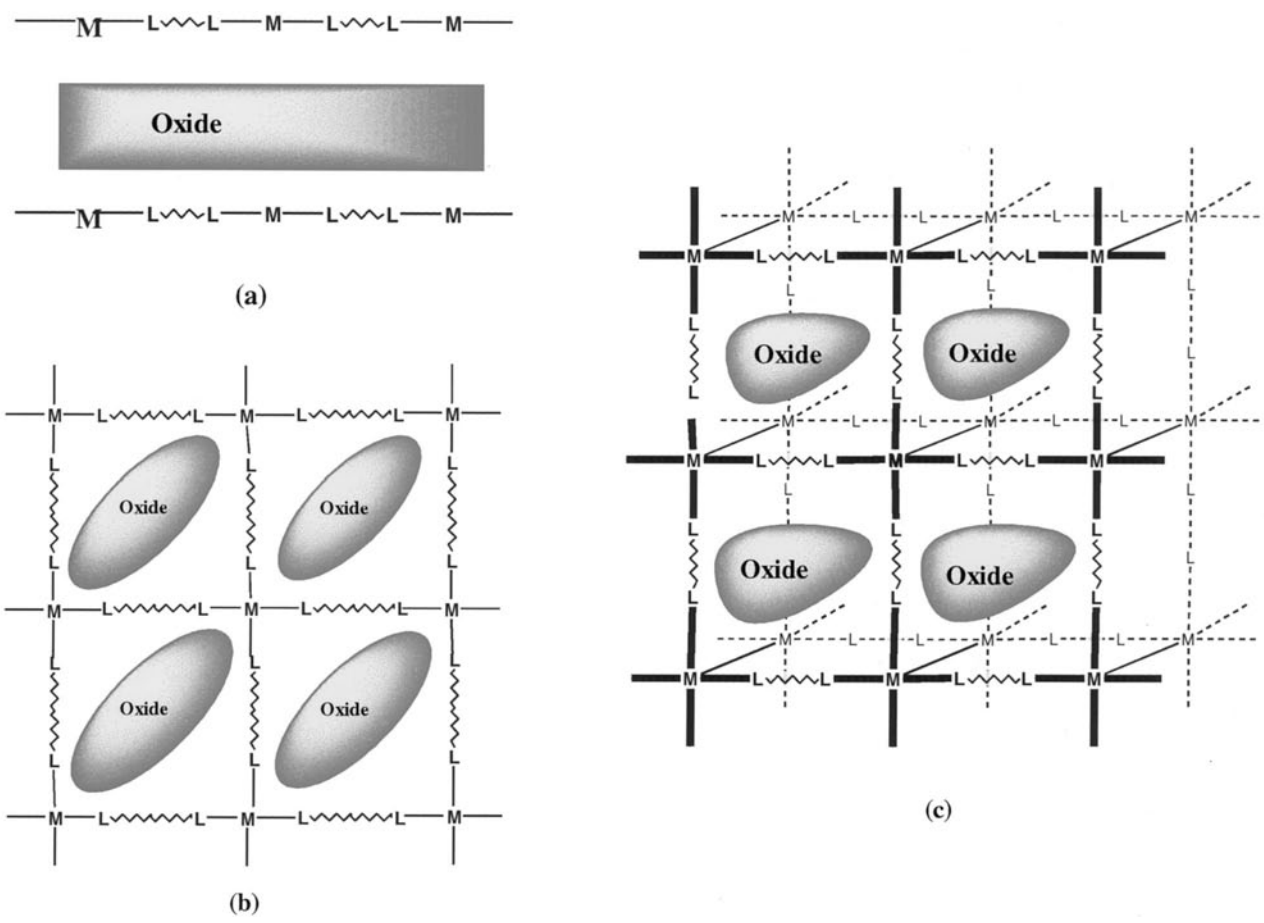

Fig. 6. Schematic views of metal oxide substructures entrained in one-, two-, and three-dimensional coordination complex cation polymers.

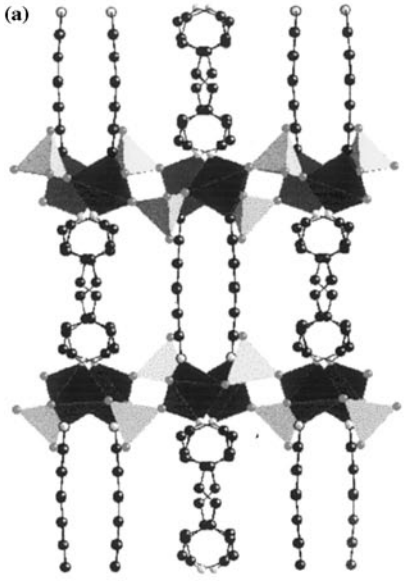

$Cu(dpe)MoO_4$

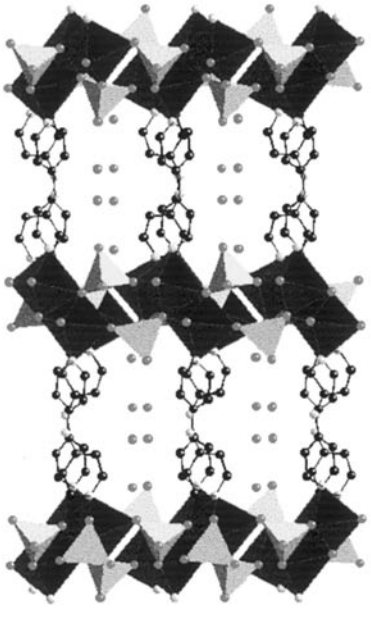

$Cu(bpa)_{0.5}MoO_4$

Fig. 7. Views of MOXI-1 and MOXI-24 (a) parallel and (b) perpendicular to the bimetallic oxide planes.

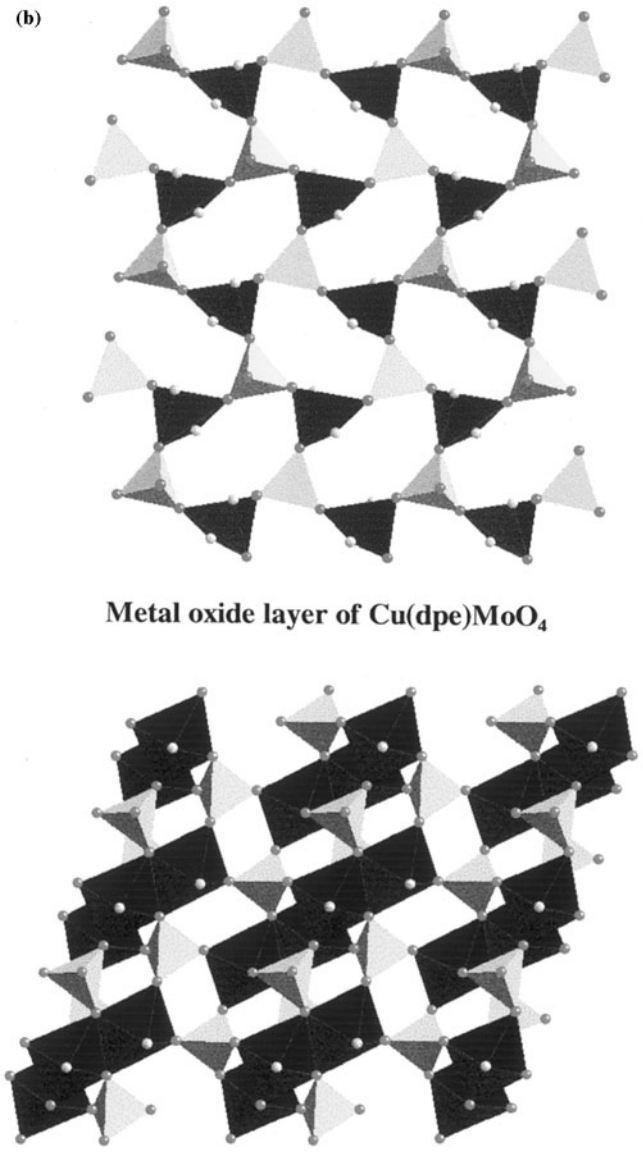

Fig. 7. (*Continued*)

The structural chemistry of this subclass of molybdenum oxides is generally complicated by the tendency of the secondary metal–amine center to link directly to the oxide substructure to give heterobimetallic oxide phases. Furthermore, the detailed geometry of the ligand may profoundly influence the structure, an observation nicely illustrated by the structures of $[Cu(bpe)MoO_4]$ (MOXI-1) and $[Cu(bpa)_{0.5}MoO_4]$ (MOXI-24), shown in Fig. 7.

The structure of MOXI-1 is constructed from $\{Cu(bpe)\}^{2+}$ linear chains bridged through $\{MoO_4\}^{2-}$ tetrahedra into a three-dimensional framework. The fundamental structural motif consists of distorted trigonal bipyramidal Cu(II) centers coordinated to two bpe ligands and three molybdate tetrahedra. The geometry at the Cu sites is defined by three oxygen donors from three $\{MoO_4\}^{2-}$ groups in the equatorial plane and two bpe nitrogen donors occupying the axial positions. Each molybdate bridges three neighboring Cu sites to produce a bimetallic oxide layer motif $\{CuMoO_4\}$. Each molybdenum site thus possesses one pendant terminal oxo group, which is directed above or below the plane. The connectivity in the plane generates 12-membered $\{Cu_3Mo_3O_6\}$ rings which fuse to propagate the layer structure. The bpe ligands extend from the metal oxide layers at an angle of ca. 35° and bridge adjacent layers to generate the overall three-dimensional covalent connectivity.

If a bend is introduced into the spacer between the pyridyl donors, not only is the donor to donor extension affected, but the entire Cu–organonitrogen subunit topology must be altered to accommodate the steric constraints imposed by the ligand. As shown in Fig. 7, the structure of $[Cu(bpa)_{0.5}MoO_4]$ (MOXI-24) consists of $\{CuMoO_4\}$ bimetallic oxide layers covalently linked through bpa ligands into a three-dimensional framework. The structure exhibits the pattern of alternating organic–inorganic regions characteristic of the metal–organophosphonate phases. The inorganic layer is constructed from $\{MoO_4\}$ tetrahedra and $\{CuO_5N\}$ octahedra which form double chains linked through $\{Cu–O–Mo\}$ bridges into a two-dimensional network. One Cu site forms corner-sharing interactions with five adjacent Mo sites of the chain, while the second Cu site forms four corner-sharing linkages to Mo chain sites and one to an Mo site of an adjacent chain. In addition, the two unique Cu sites form a binuclear edge-sharing unit through a $\{Cu_2O_2\}$ interaction. One Mo site bridges three Cu binuclear units of a given chain and provides linkage to an adjacent chain through its fourth oxo-group. The second Mo site bridges three Cu binuclear units of the chain and projects a terminal oxo-group into the interlamellar region. Most significantly, the copper–organonitrogen structural motif is binuclear and terminated by copper–oxygen bonding, thus precluding extension into a one-dimensional motif.

Another obvious expedient in ligand design is the contraction of the donor-to-donor distance, a feature manifested in the structures of $[Cu(pyrazine)_{0.5}MoO_4]$ (MOXI-25) and $[Cu_2(pyrimidine)Mo_3O_{10}]$ (MOXI-19), shown in Fig. 8. The structure of MOXI-25 consists of a complex three-dimensional bimetallic oxide with channels occupied by the pyrazine ligand. The structure is constructed from corner-sharing $\{MoO_4\}$ tetrahedra and $\{CuO_4N\}$ square pyramids, which form chains of stacked $\{Cu_2Mo_2O_4\}$ rings. Each Mo site links three adjacent Cu sites of a chain and employs the fourth oxo-groups to connect to an adjacent chain. Four adjacent chains are linked to form a cavity occupied by the pyrazines which serve to ligate to Cu sites of opposite chains of the channel.

The consequences of introducing pyrimidine into the Cu–molybdenum oxide chemistry are quite unanticipated. The structure of $[Cu_2(pyrd)Mo_3O_{10}]$ (MOXI-19) is constructed from $\{MoO_6\}$ octahedra and $\{CuO_3N\}$ tetrahedra, which link to

form a three-dimensional bimetallic oxide framework with channels occupied by the pyrimidine groups. The $\{MoO_6\}$ octahedra form a chain of edge-sharing polyhedra, structurally analogous to that observed for the one-dimensional $(NH_4)_2[Mo_3O_{10}]$. Each Cu site coordinates to two oxo-groups of two Mo sites of one chain and bridges an adjacent chain by bonding to one oxo-group. In addition, each Cu center coordinates to a nitrogen donor of a pyrimidine ligand, which serves to bridge to a second Cu site through its second nitrogen donor. When viewed along the crystallographic *a* axis, the Mo-oxide chains are linked through stacked $\{CuO_3N\}$ tetrahedra to produce channels of sufficient diameter to accommodate parallel stacks of pyrimidine groups.

It is noteworthy that crystals of MOXI-19 are black, indicative of mixed valence, the only example to date for this class of materials. Valence sum calculations provide an average oxidation state of $+5.7$ for the Mo sites; curiously, the Cu sites exhibit an average oxidation state of $+1.5$, suggesting extensive electronic delocalization.

6. Cationic matrices: the three connect ligand and 'ship in the bottle' design

The constraints imposed by the ligand geometry are reflected in the variety of motifs adopted by the copper–organonitrogen substructures, which include chains, virtual two-dimensional networks and binuclear units. However, no three-dimensional cationic frameworks have been observed to date for the dipodal organonitro-

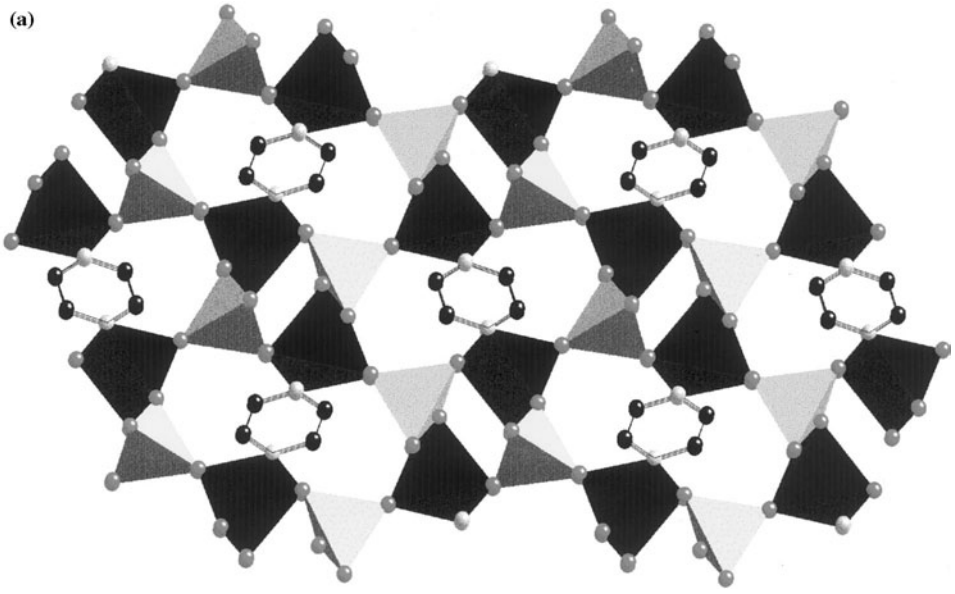

Fig. 8. The structures of (a) MOXI-25 and (b) MOXI-19.

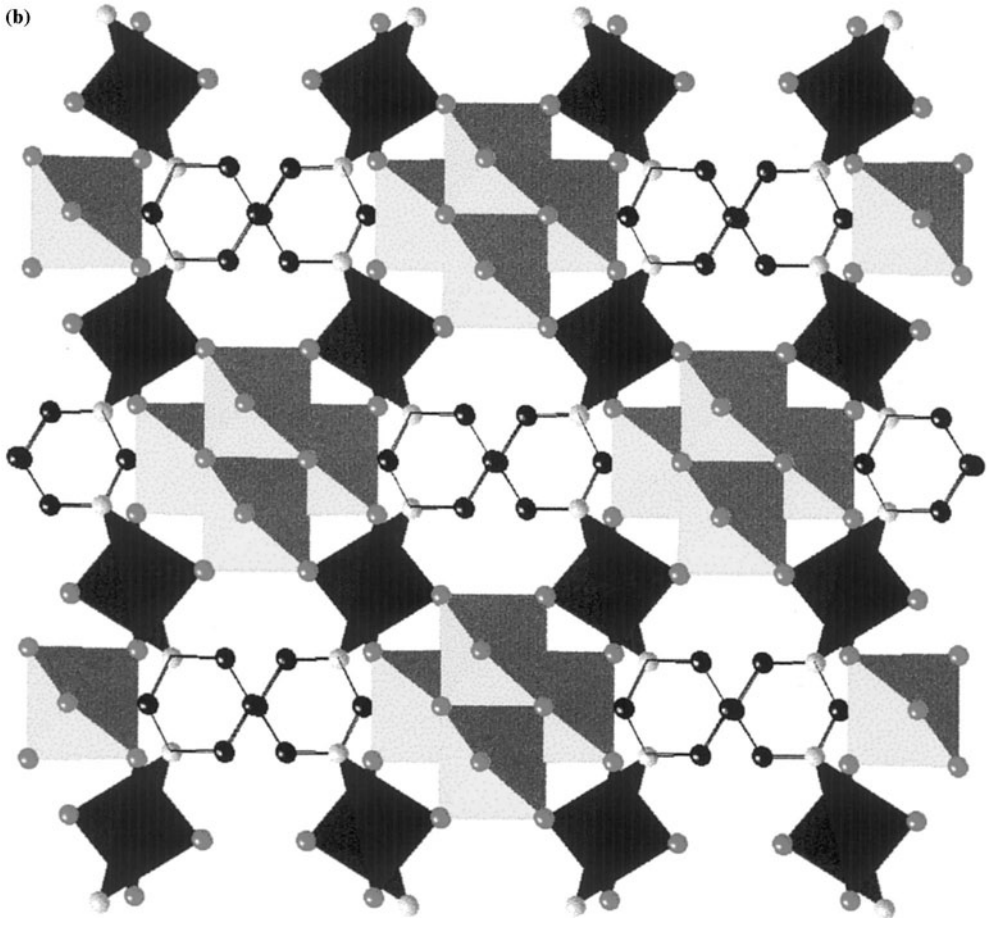

Fig. 8. (*Continued*)

gen ligand types. However, the work of Robson [29] and Ciani [30] on M(II)-organonitrogen framework architectures suggested that tripodal ligands or higher denticity donors would more readily provide a three-dimensional Cu–organonitrogen cationic framework. This expectation has been realized in the structure of $[Cu_2(triazolate)_2(H_2O)_2Mo_4O_{13}]$ (MOXI-26), shown in Fig. 9. The structure consists of $\{Mo_4O_{13}\}^{2-}$ one-dimensional chains entrained within the complex three-dimensional framework of the $\{Cu_2(triazolate)_2(H_2O)_2\}^{2+}$ cationic substructure. There are two distinct Cu(II) sites. One coordinates to four nitrogen donors from four bridging triazolate ligands, forming a $\{Cu(triazolate)\}_n^{n+}$ chain, and to two oxygen atoms of two adjacent molybdate chains. The second copper site coordinates to the apical nitrogen of the triazole ligand, serving to link the $\{Cu(triazolate)\}_n^{n+}$ chains into a three-dimensional framework. In addition, this copper center binds to two aquo ligands and to two oxygen atoms from adjacent

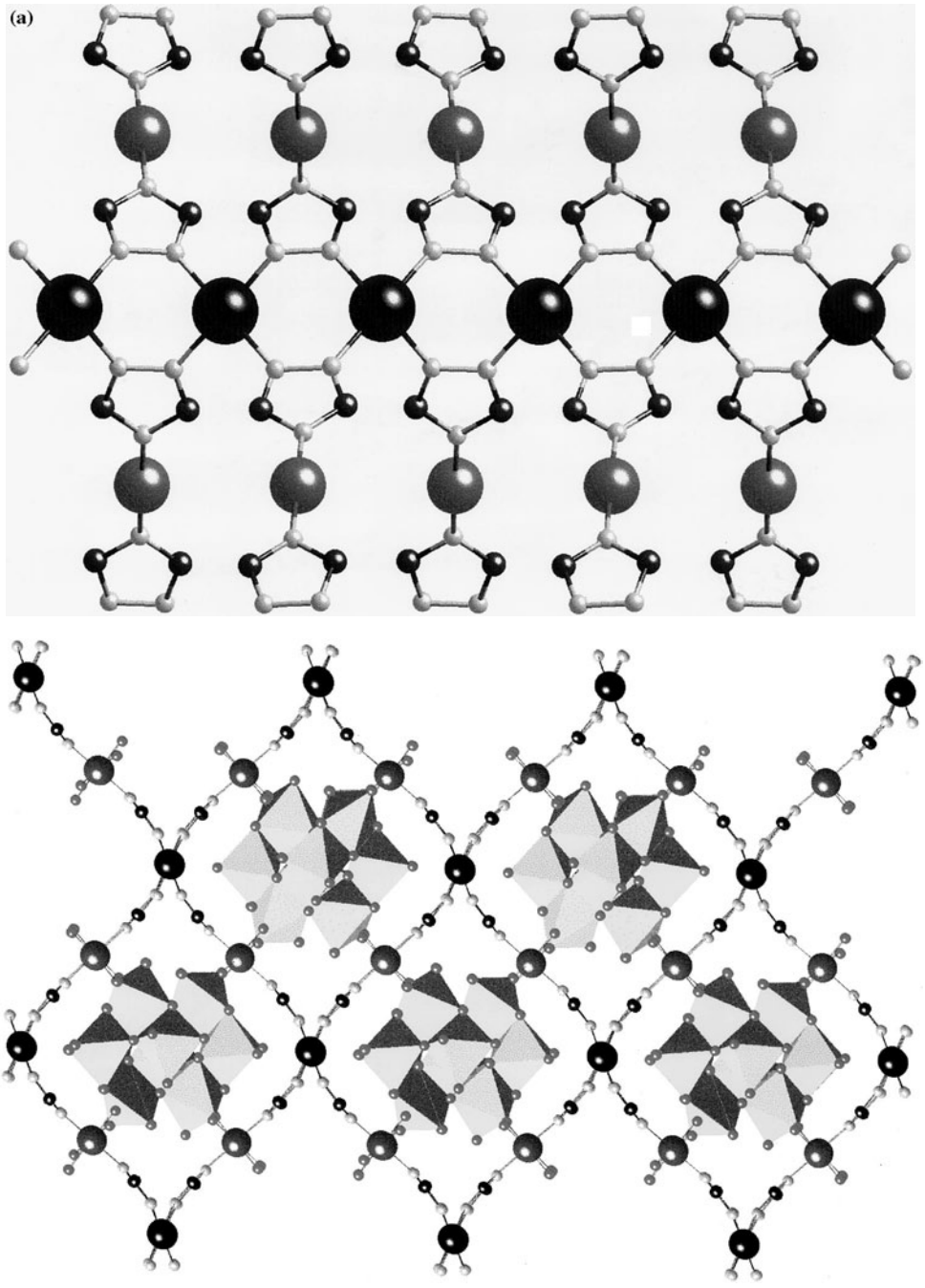

Fig. 9. (a) The cationic framework of MOXI-26. (b) A view of the structure of MOXI-26 showing the entraining of the molybdate chains in the cationic framework.

molybdate chains. The structure of the molybdate is distinct from those previously reported for one-dimensional molybdate chains, reflecting the constraints imposed by the cationic framework.

In extending the concept of the three-connect Cu-triazolate framework to the vanadium oxides, it was naively assumed that the constraints imposed by the cationic scaffolding would encapsulate one-dimensional vanadium oxide substructures rather than the more common two-dimensional motifs. However, it is apparent that the oxide subunit behaves not as a ship-in-the-bottle but rather as a synergistically active component of the composite, such that the product $[\{Cu_3(triazolate)_2\}V_4O_{12}]$ exhibits one-dimensional vanadate chains entrained within an unexpected Cu-triazolate two-dimensional network, shown in Fig. 10. The structure consists of a three-dimensional covalent framework constructed from two dimensional $\{Cu_3(triazolate)_2\}_n^{4n+}$ networks linked through one-dimensional $\{VO_3\}_n^{n-}$ chains. The cationic network when viewed parallel to [001] displays a pronounced sinusoidal ruffling with an amplitude of about 4.75 Å and a period of 8.87 Å. The layers are composed of Cu(II) sites digonally coordinated through triazolate ligands, each of which bridges three copper sites. Within each layer, there are large rhombic rings, $\{Cu_6(triazolate)_6\}$, which form the distinctive lattice-work motif with each ring sharing an edge with six adjacent rings.

7. Phases constructed from organically templated metal halides and pseudohalides

Encouraged by the extensive structural chemistry induced by the introduction of organic components into metal oxide substructures, an investigation of metal halide and pseudohalide solids was initiated. That similar strategies may be exploited is validated by the structure of $[\{Cu(en)_2\}_2Cu_7Cl_{11}]$, shown in Fig. 11.

The framework of this material is constructed from disordered Cu_6 hexanuclear building blocks which contain copper tetrahedrally coordinated by chloride ligands. The units, composed of edge sharing $CuCl_4$ tetrahedra, are linked into a covalently bonded three-dimensional lattice by three coordinate Cu atoms. The three-dimensional copper halide framework can be conceptually envisioned as being built up in space group $P4_2nm$ from the aforementioned units connected along the 4_2 screw axis via the trigonal $CuCl_{3/3}$ bridges into rectangular spirals. These spirals are in turn intertwined with another crystallographically identical spiral to give copper halide double helices. This connectivity generates voids in the framework that are filled by charge compensating $[(en)_2Cu]^{2+}$ cations.

The influences of ligand geometry and steric bulk may also be considerable. The three-connect triazolate ligand encourages the formation of three-dimensional frameworks, as shown in Fig. 12 for $[Cu_2Br_2(trz)]$. The structure is constructed from chains of edge-sharing $\{CuBr_4N_2\}$ octahedra linked through trigonal planar $\{CuBr_2N\}$ sites into a two-dimensional network. The triazolate ligands which serve to bridge the octahedral sites through the 1,2-nitrogen donor sites project into the interlamellar region and employ the third nitrogen donor to bond to the trigonal

site of an adjacent layer. The triazolate ligands consequently link the copper–bromide layers into a three-dimensional organic–inorganic composite.

Bulky ligands may introduce steric constraints which serve to passivate the metal with respect to bridging linkages and consequently to favor lower dimensionality materials, an observation reflected in the structures of $[CuBr_2(bpy)]$ and $[Cu_2(OH)_2$-

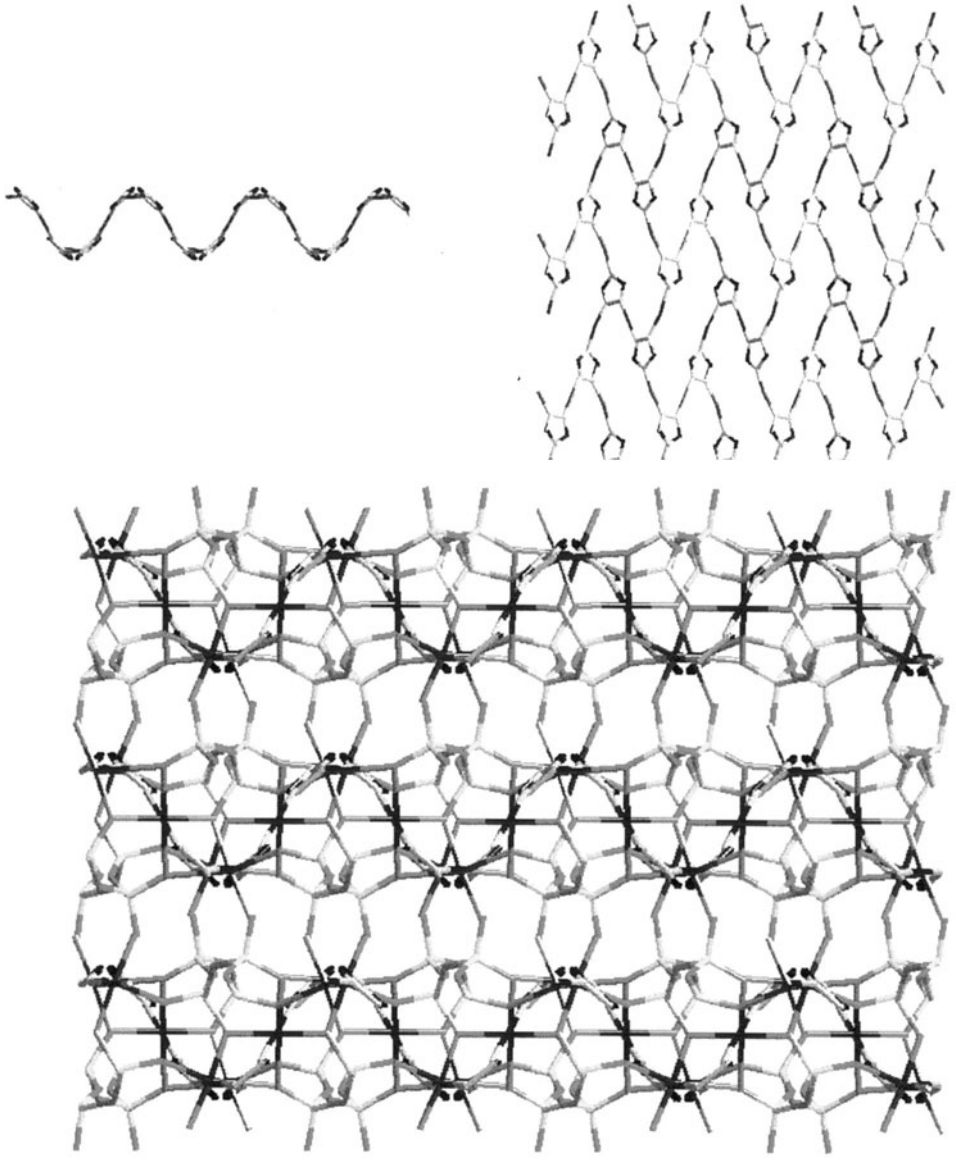

Fig. 10. (a) The cationic network of $[Cu_3(triazolate)_2V_4O_{12}]$, edge-on showing the sinusoidal ruffling, and projected onto the page. (b) The threading of the vanadate chains through the cationic network.

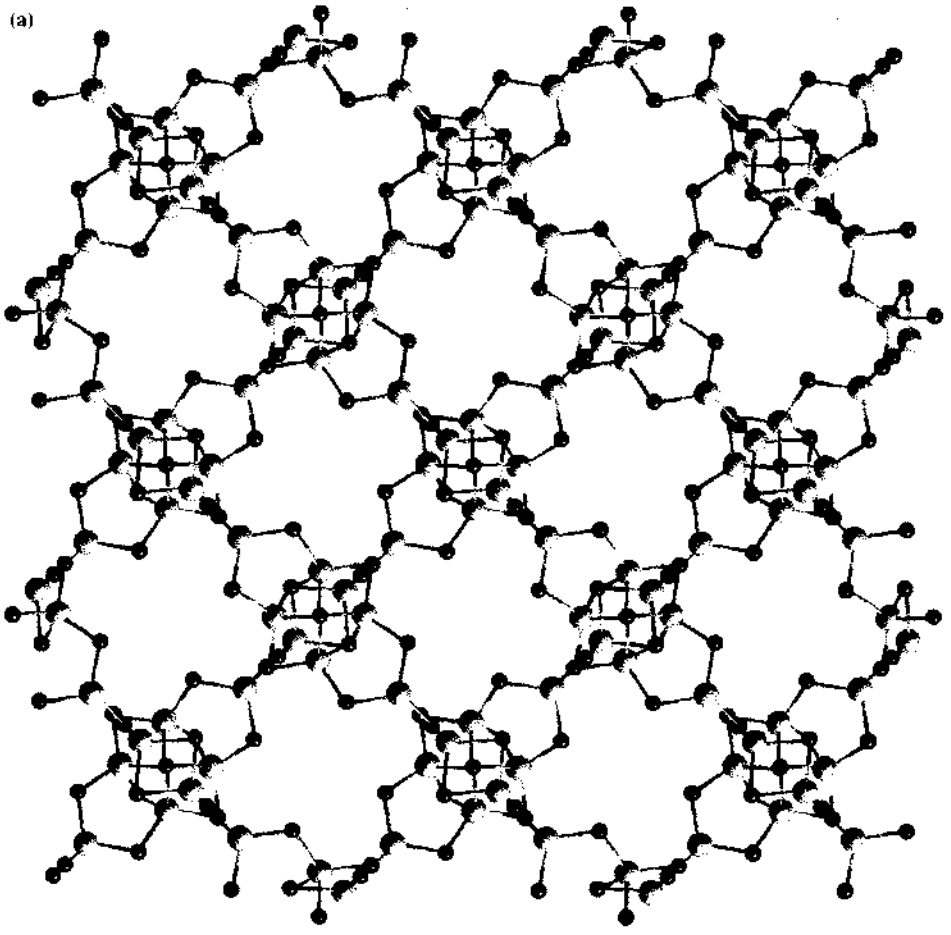

Fig. 11. (a) A view of the structure of $[\{Cu(en)_2\}_2Cu_7Cl_{11}]$. (b) The fundamental building block.

$(bpy)_2][Cu_4Br_6]$, shown in Fig. 13. The one-dimensional structure of $[CuBr_2(bpy)]$ consists of a chain of *cis*-edge-sharing $\{CuBr_4N_2\}$ octahedra. In contrast, the structure of $[Cu_2(OH)_2(bpy)_2][Cu_4Br_6]$ is constructed from $\{Cu_4Br_6\}^{2-}$ chains linked through $[Cu_2(OH)_2(bpy)_2]^{2+}$ units into a two-dimensional network.

The rich supramolecular chemistry of the metal derivatives of the pseudohalide cyanide ligand [31] encouraged us to expand our investigations to the copper–cyanide–organoamine family of materials, exploiting the bridging cyano ligand as a rigid tether in the propagation of Cu(I) geometry in solid state materials. The structural diversity of this system is illustrated by the structures of $[\{Cu_2(bpy)_2(CN)\}Cu_5(CN)_6]$ (CUNC-1) and $[\{Cu_2(bpy)_2(CN)\}Cu_5(CN)_7]$ (CUNC-2), shown in Fig. 14. The structure of CUNC-1 consists of sheets of fused 36 membered puckered honeycomb rings interpenetrated by $[Cu_2(bpy)_2(CN)]^{+1}$ cations. The rings are composed of two nearly linear $\{Cu(CN)_2\}$ sites, four bent

{$Cu(CN)_2$} moieties and six {$Cu(CN)_3$} distorted trigonal planar sites which serve as junctions between adjacent rings. Each ring is interpenetrated by two space-filling and charge compensating $[Cu_2(bpy)_2(CN)]^{+1}$ cations at an oblique angle to the {Cu(CN)Cu} axis of the cation with respect to the face of the ring. The honeycomb layers are offset along the stacking axis *b*, so as to generate channels of approximate dimensions 5.4 × 9.0 Å which are occupied by the cations. Each cation interpenetrates rings from two adjacent layers, which are separated by 3.5 Å. While two-dimensional Cu–CN networks have been observed for $[Cu_3(en)_2(CN)_4]\cdot 6H_2O$ [32] and $K[Cu_2(CN)_3]\cdot H_2O$ [33], the layers are constructed from significantly smaller 15- and 18-membered rings.

The $[Cu_5(CN)_7]^{2-}$ network of CUNC-2 exhibits a honeycomb motif distinct from that of CUNC-1. The network is constructed from rows of fused 18- and 24-membered rings in a nearly planar arrangement. The $\{Cu_2(bpy)_2(CN)\}^{+1}$ cations occupy the interlamellar region and, in contrast, to the cations of CUNC-1 do not penetrate the layers.

The unique role of triazole as a three-connect ligand for framework construction may also be incorporated into the metal–pseudohalide structural chemistry. As manifest in the structure of $[Cu_3(CN)_2(triazolate)(bpy)]$ (CUNC-3) and $[Cu_6(CN)_4(triazolate)_2(bpy)]$ (CUNC-4), the bpy ligand serves to passivate the metal

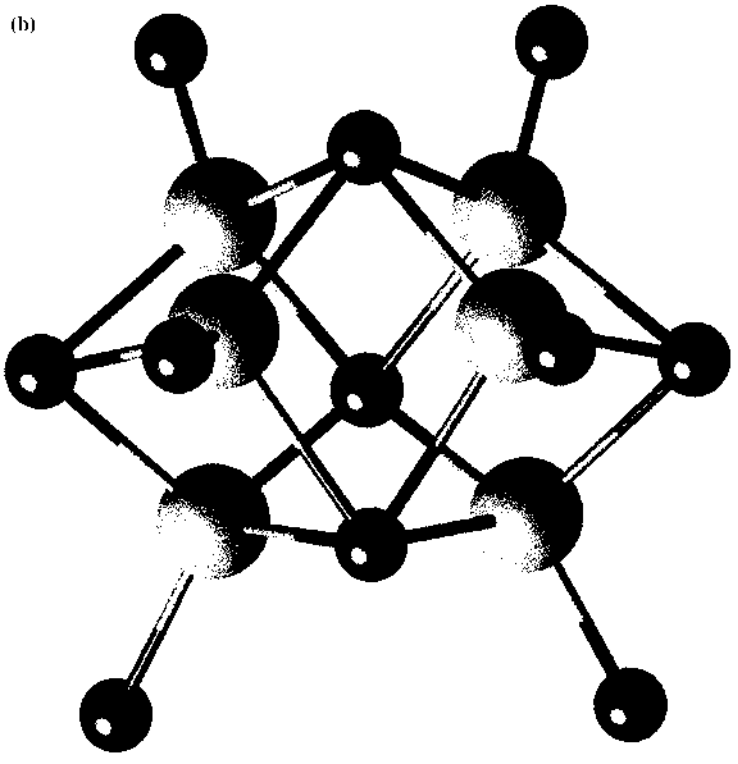

Fig. 11. (*Continued*)

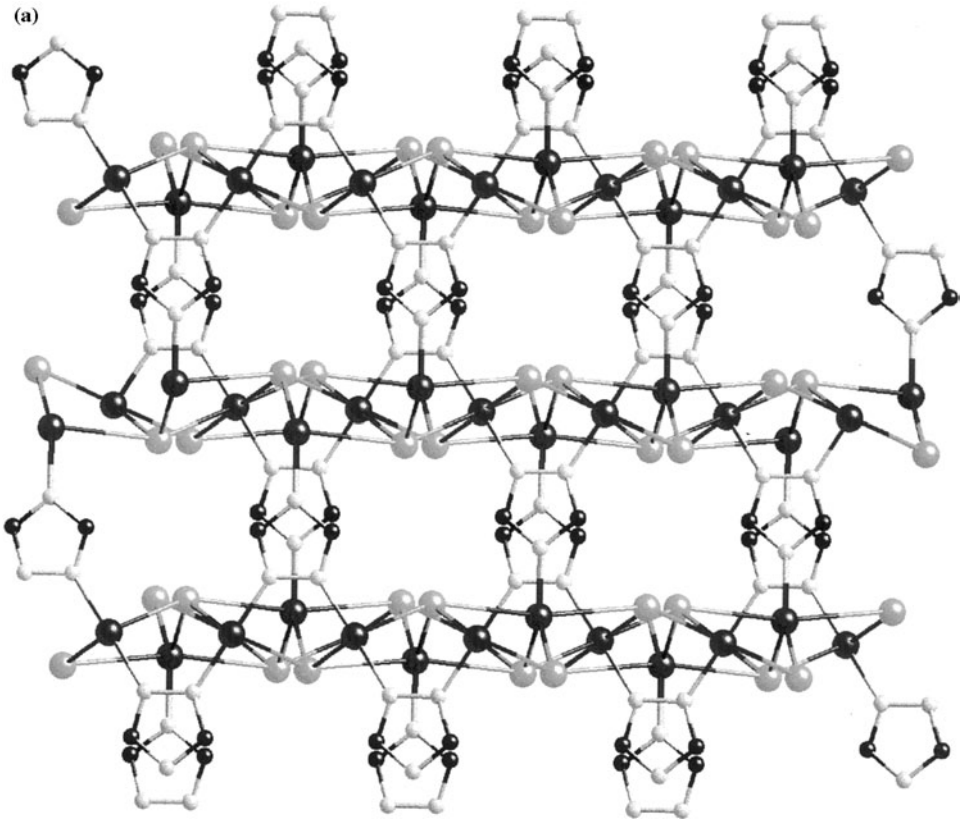

Fig. 12. Views of the structure of $[Cu_2Br_2(triazolate)]$: (a) showing the linking of $\{Cu_2Br_2\}^{+}$ layers through triazolate bridges and (b) a view of a single layer illustrating the chains of $\{CuBr_4N_2\}$ octahedra linked through trigonal planar $\{CuBr_2N\}$ centers.

with respect to additional bridging interactions, resulting in lower-dimensionality structures. The ribbon structure of CUNC-3 is constructed from binuclear $\{Cu_2(triazolate)_2\}$ units wherein the Cu(I) sites are bridged through the 1,2-nitrogen donors of the triazolate ligand. The nitrogen at the 4-position of the triazolate bonds to a $\{Cu(CN)_2\}^{1-}$ group which serves to link two adjacent $\{Cu_2(triazolate)_2\}$ units and to a single $\{Cu(bpy)\}^{+1}$ motif which functions as a chain terminating unit, preventing further association in a second dimension (Fig. 15).

The $\{Cu_2(triazolate)_2\}$ motif is also observed in the structure of CUNC-4. However, the binuclear units are linked through $\{Cu(CN)_2\}^{-1}$ units bonded to the nitrogen donor at the 4-position of one triazolate ligand and through a digonal copper site bonded to the nitrogen donors of triazolate units from two adjacent binuclear groups. The result is a network structure constructed from 26- and 30-membered rings. Aggregation into a three-dimensional framework appears to be blocked by the {Cu(bpy)(CN)} units which link to one copper site of each binuclear unit and project into the interlamellar region.

8. Conclusions

The ability of organic molecules to alter inorganic microstructures offers a powerful technique for the design of new materials. In such applications it appears that the role of the organic component is not limited to that of leaving a molecular sized void in the framework upon post-synthesis removal, as in the case of zeolitic materials, but extends to an essential synthetic function by providing a species that can allow the crystal to grow via charge neutralization at the crystal–solution interface by virtue of possessing a suitable shape and charge to volume ratio. Such incorporation of an organic molecule will necessarily induce a large degree of structural complexity into the system by virtue of the relatively large number of skeletal atoms required to accommodate a large organic component. This general strategy finds a logical elaboration in the introduction of structural subunits consisting of coordination complex cations, which are incorporated into the anionic metal–oxide or metal–halide substructure.

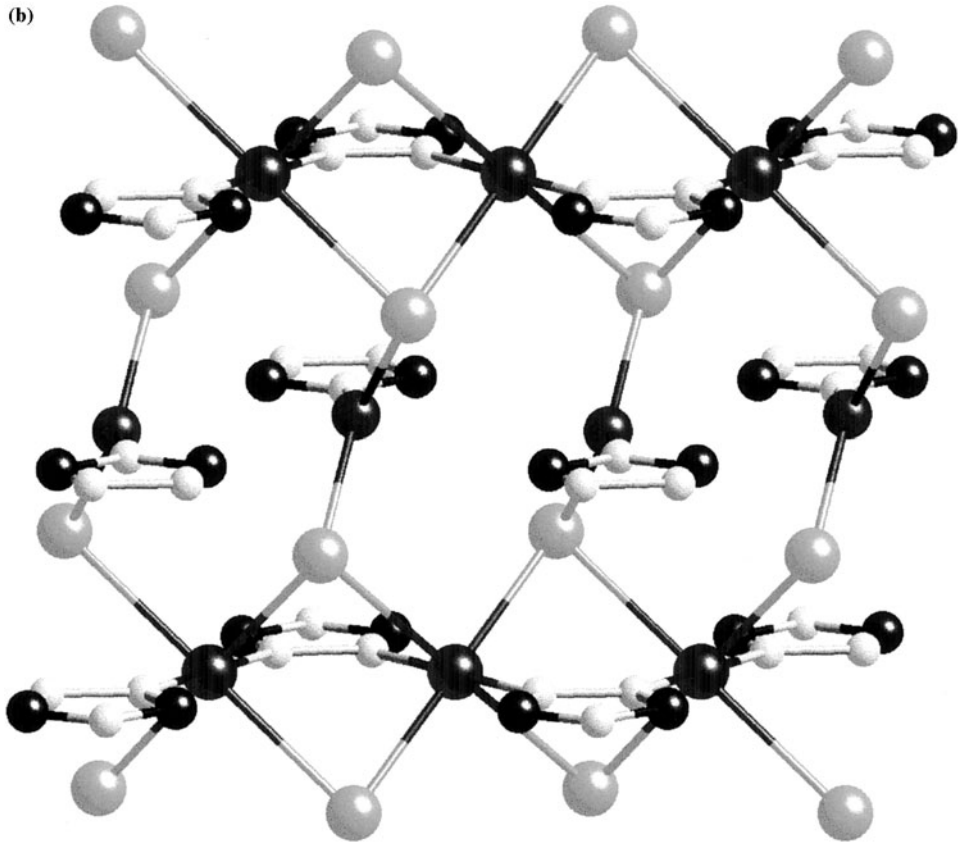

Fig. 12. (*Continued*)

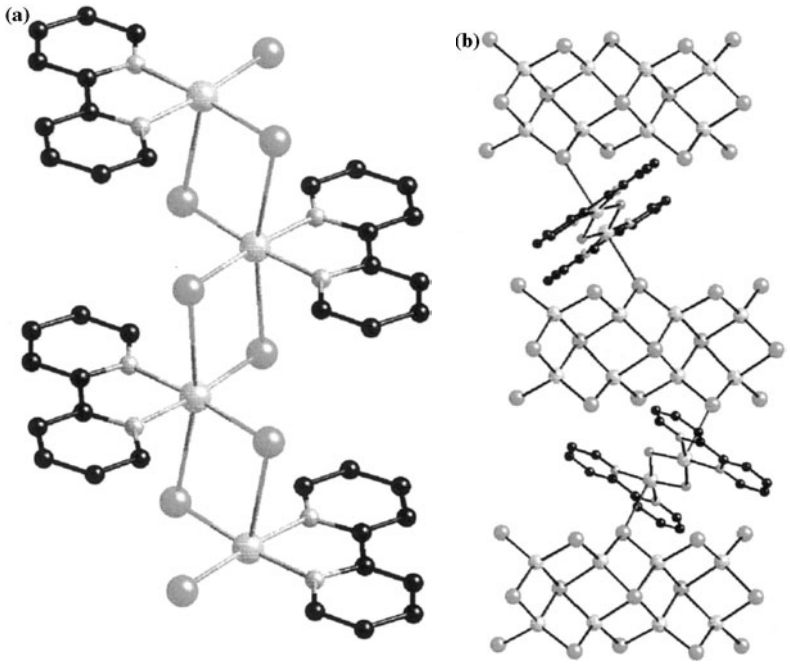

Fig. 13. The structures of (a) $[CuBr_2(bpy)]$ and (b) $[Cu(OH)_2(bpy)_2][Cu_4Br_6]$.

By employing bridging ligands of specific geometric design, coordination complex polymeric cations which impose various geometric constraints on the anionic substructure may be conceived. However, the structures described in this review belie the naive ship-in-the-bottle construct, wherein the engineered cationic substructure provides a rigid matrix for the isolation of the metal oxide or halide motif, but rather suggest a synergism between the oxide and cationic coordination complex polymer at the organic–inorganic interface. While the approach of introducing the appropriate metal cation and ligand to accomplish the self-assembly of a polymeric cationic substructure has allowed a more or less predictable approach to the isolation of low dimensional oxide and halide subunits, absolute synthetic control in the sense of crystal engineering remains elusive. Such composite materials are metastable phases, crystallizing under nonequilibrium conditions from a complex hydrothermal domain. We are currently exploring the use of preformed cationic networks and frameworks and of oxide clusters and the exploitation of non-hydrothermal conditions as synthetic approaches.

Acknowledgements

This work was supported by a grant from the National Science Foundation (CHE9617232).

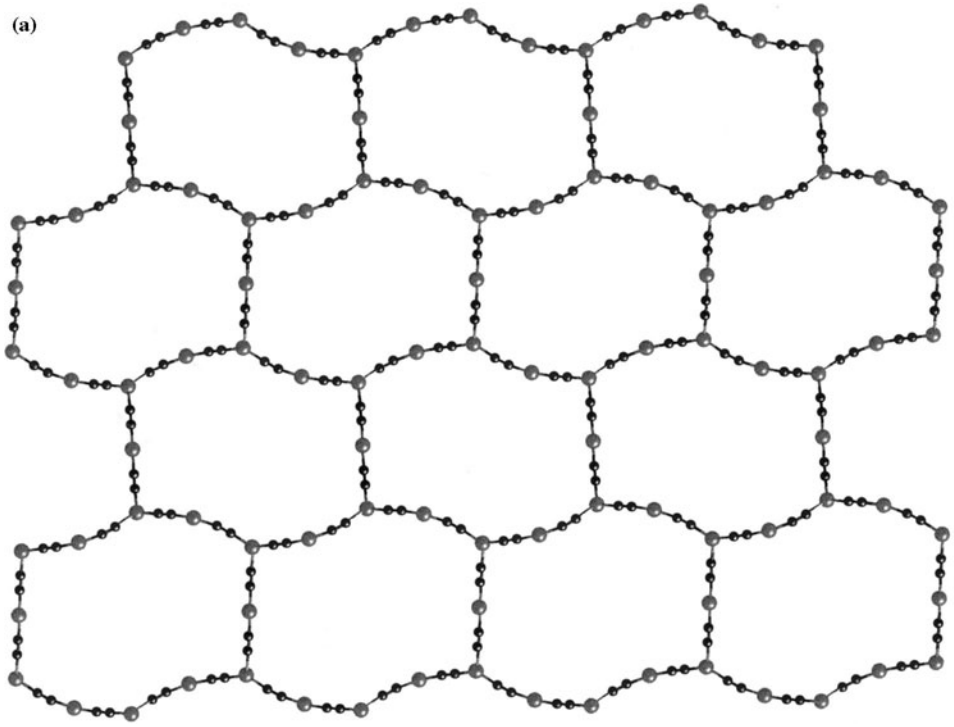

Fig. 14. The two-dimensional networks of (a) CUNC-1 and (b) CUNC-2. (c) A view of the threading of the $\{Cu_2(bpy)_2(CN)\}^{1+}$ cations through the anionic network of CUNC-1.

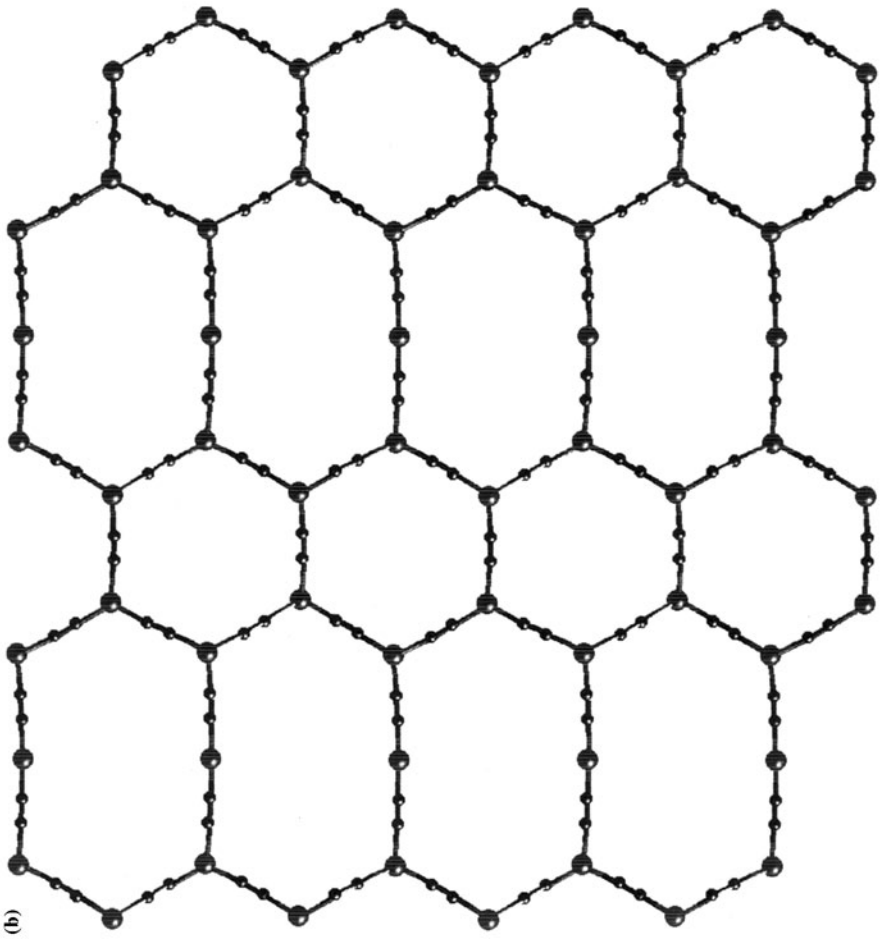

Fig. 14. (*Continued*)

Fig. 14. (*Continued*)

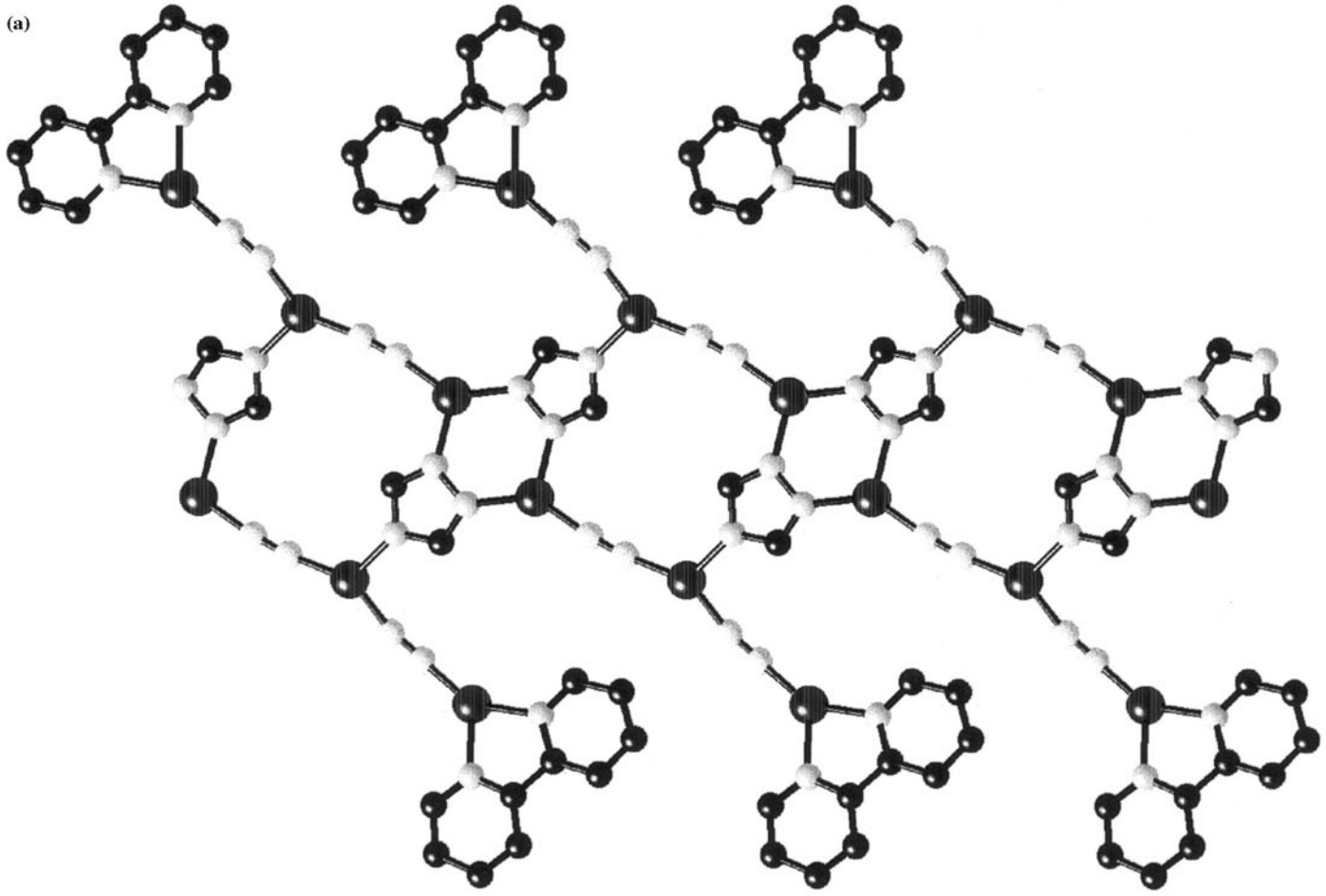

Fig. 15. (a) The one-dimensional chain of CUNC-3. (b) The two-dimensional network of CUNC-4. (c) The location of the passivating {CuCN(bpy)} units relative to the layer of CUNC-4.

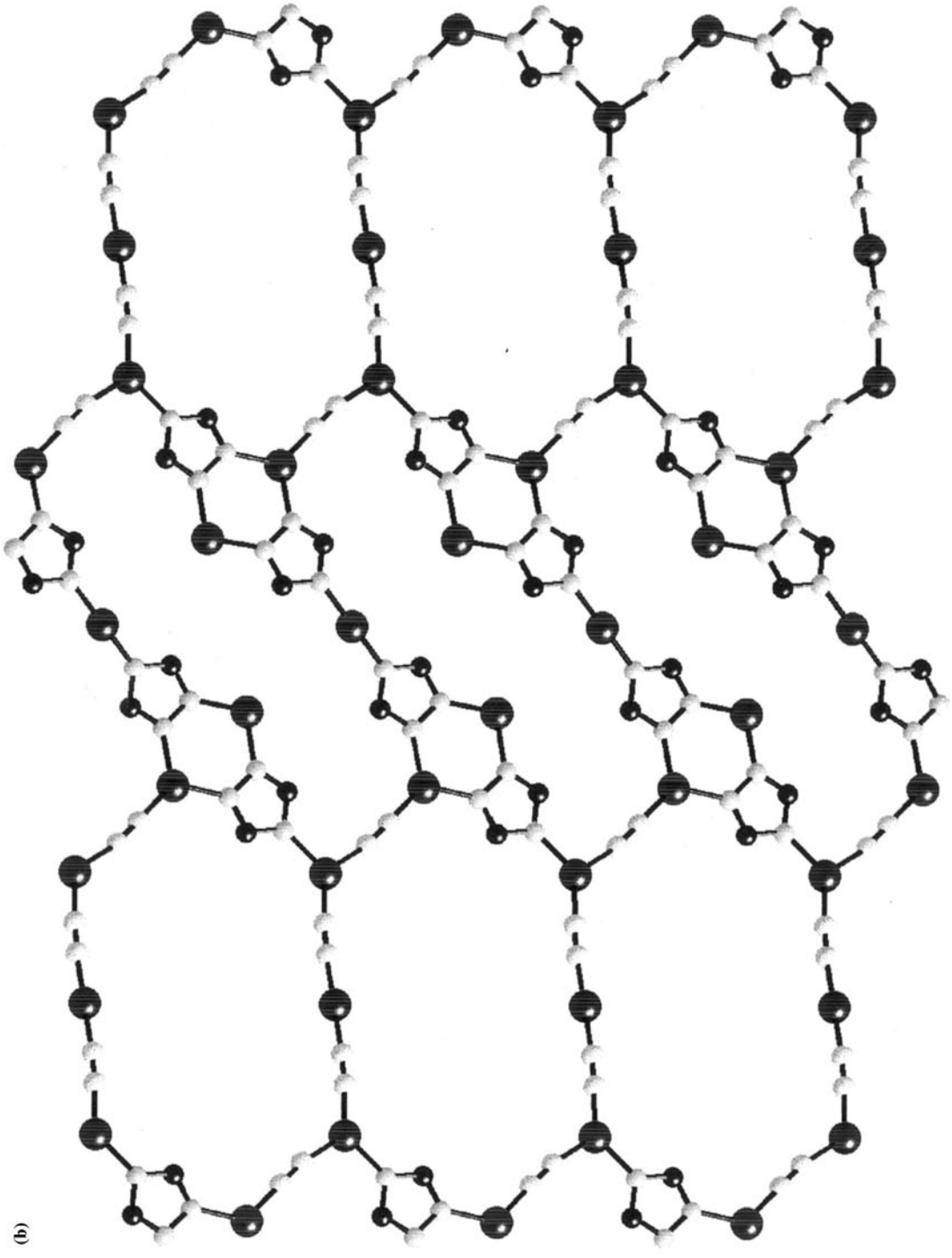

Fig. 15. (*Continued*)

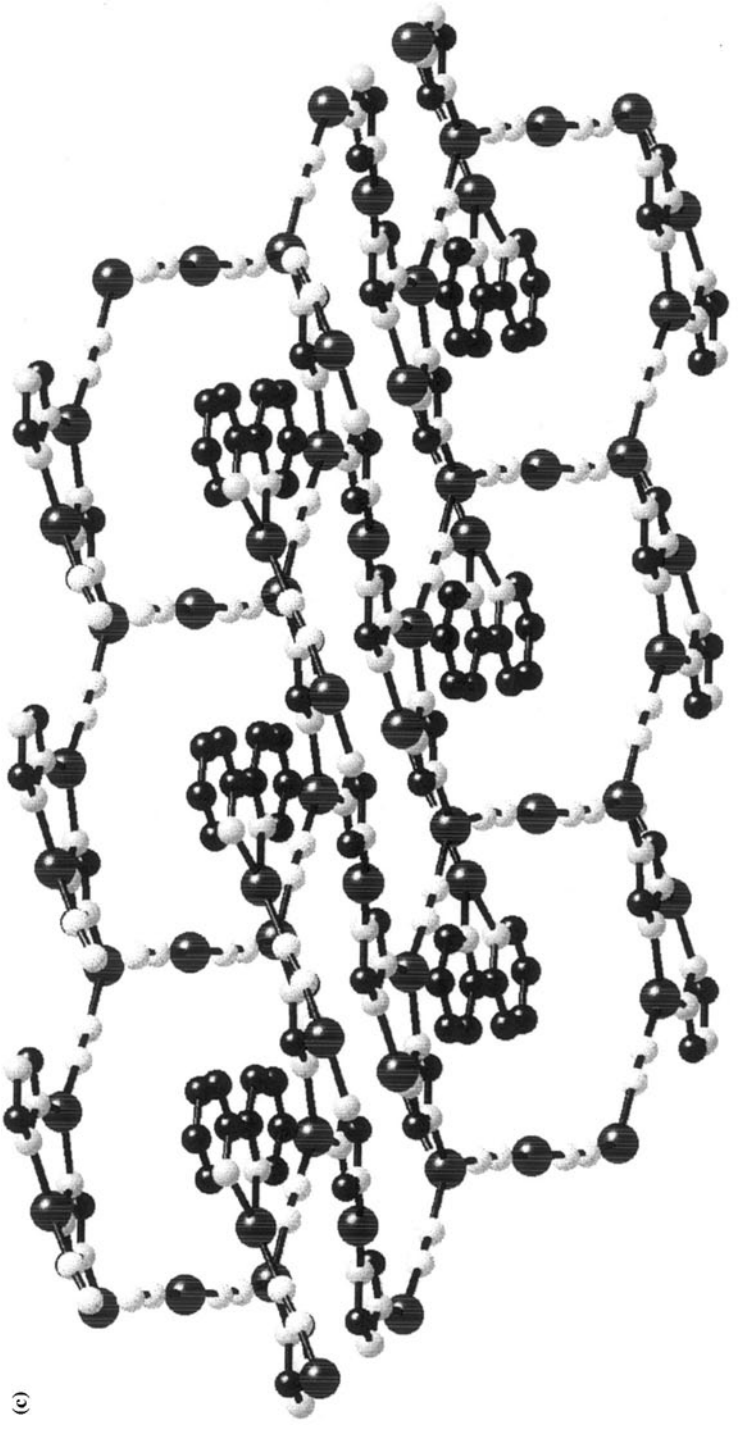

Fig. 15. (*Continued*)

References

[1] A.K. Cheetham, Science 264 (1994) 794.
[2] S. Mann, J. Chem. Soc. Dalton Trans. (1997) 3953.
[3] S. Mann, G.A. Ozin, Nature (Lond.) 382 (1996) 313.
[4] (a) J.V. Smith, Chem. Rev. 88 (1988) 149. (b) M.L. Occelli, H.C. Robson, Zeolite Syntheses, American Chemical Society, Washington, DC, 1989.
[5] C.T. Kresge, M.E. Leonowicz, W.J. Roth, J.C. Vartuli, J.S. Beck, Nature 359 (1992) 710.
[6] S. Mann, Nature 365 (1993) 499.
[7] R.C. Haushalter, L.A. Mundi, Chem. Mater. 4 (1992) 31.
[8] V. Soghomonian, Q. Chen, R.C. Haushalter, J. Zubieta, C.J. O'Connor, Science 259 (1993) 1596.
[9] M.I. Khan, L.M. Meyer, R.C. Haushalter, C.L. Schweitzer, J. Zubieta, J.L. Dye, Chem. Mater. 8 (1996) 43.
[10] D. Hagrman, C. Zubieta, D.J. Rose, J. Zubieta, R.C. Haushalter, Angew. Chem. Int. Ed. Engl. 36 (1997) 795.
[11] P.J. Zapf, R.C. Haushalter, J. Zubieta, Chem. Mater. 9 (1997) 2019.
[12] P.J. Zapf, C.J. Warren, R.C. Haushalter, J. Zubieta, Chem. Commun. (1997) 1543.
[13] D. Hagrman, R.C. Haushalter, J. Zubieta, Chem. Mater. 10 (1998) 361.
[14] P.J. Zapf, R.P. Hammond, R.C. Haushalter, J. Zubieta, Chem. Mater. 10 (1998) 1366.
[15] D. Hagrman, C.J. Warren, R.C. Haushalter, R.S. Rarig Jr., K.M. Johnson III, R.L. LaDuca Jr., J. Zubieta, Inorg. Chem. 37 (1998) 3411.
[16] D. Hagrman, P.J. Zapf, J. Zubieta, Chem. Commun. (1998) 12830.
[17] D. Hagrman, R.P. Hammond, R.C. Haushalter, J. Zubieta, Chem. Mater. 10 (1998) 3294.
[18] M.I. Khan, J. Zubieta, Prog. Inorg. Chem. 43 (1995) 1.
[19] A. Rabenau, Angew. Chem. Int. Ed. Engl. 24 (1985) 1026.
[20] R.A. Laudise, Chem. Eng. News Sept. 28 (1987) 30.
[21] J. Gopalakrishnan, Chem. Mater. 7 (1995) 1265.
[22] See for example: G. Huan, A.J. Jacobson, J.W. Johnson, E.W. Corcoran Jr., Chem. Mater. 2 (1990) 91.
[23] J. Fuchs, S. Mahjour, J. Pickhardt, Angew. Chem, Int. Ed. Engl. 15 (1976) 374.
[24] Y. Zhang, P.J. Zapf, L.M. Meyer, R.C. Haushalter, J. Zubieta, Inorg. Chem. 36 (1997) 2159.
[25] J.R.D. DeBord, R.C. Haushalter, C.M. Meyer, D.J. Rose, P.J. Zapf, J. Zubieta, Inorg. Chim. Acta 256 (1997) 165.
[26] D. Hagrman, R.C. Haushalter, J. Zubieta, unpublished results.
[27] See for example: (a) R. Robson, in: J.L. Atwood, J.E.D. Davies, D.D. MacNicol, F. Vögtle, J.-M. Lehn (Eds.), Comprehensive Supramolecular Chemistry, vol. 6, Pergamon, New York, 1996, pp. 733. (b) K.N. Power, T.L. Hennigar, M.J. Zaworotko, Chem. Commun. (1998) 595. (c) B.F. Hoskins, R. Robson, D.A. Slizys, Angew. Chem. Int. Ed. Engl. 36 (1997) 2336. (d) M.A. Withersby, A.J. Blake, N.R. Champness, P. Hubberstey, W.-S. Li, M. Schröder, Angew. Chem. Int. Ed. Engl. 36 (1997) 2327. (e) S. Lopez, M. Kahraman, M. Harmata, S.W. Keller, Inorg. Chem. 36 (1997) 6138. (f) L. Carlucci, G. Ciani, D.M. Proserpio, A. Sironi, J. Chem. Soc. Dalton Trans. (1997) 1801.
[28] See for example: (a) P. Losier, M.J. Zaworotko, Angew. Chem. Int. Ed. Engl. 35 (1996) 2779. (b) O.M. Yaghi, H. Li, T.L. Groy, Inorg. Chem. 36 (1997) 4292. (c) N. Masciocchi, P. Cairati, L. Carlucci, G. Mezza, G. Ciani, A. Sironi, J. Chem. Soc. Dalton Trans. (1996) 2739. (d) F. Robinson, M.J. Zaworotko, J. Chem. Soc. Chem. Commun. (1995) 2413. (e) O.M. Yaghi, H. Li, J. Am. Chem. Soc. 118 (1996) 295. (f) M. Kondo, T. Yoshitomi, K. Seki, H. Matsuzaka, S. Kitagawa, Angew. Chem. Int. Ed. Engl. 36 (1997) 1725. (g) O.M. Yaghi, G. Li, Angew. Chem. Int. Ed. Engl. 34 (1995) 207. (h) L. Carlucci, G. Ciani, D.M. Proserpio, A. Sironi, J. Chem. Soc. Chem. Commun. (1994) 2755. (i) L.R. MacGillivray, S. Subramamian, M.J. Zaworotko, J. Chem. Soc. Chem. Commun. (1994) 1325.
[29] (a) B.F. Abrahams, P.A. Jackson, R. Robson, Angew. Chem. Int. Ed. Engl. 37 (1998) 2656. (b) S.R. Batten, R. Robson, Angew. Chem. Int. Ed. Engl. 37 (1998) 1461 and references therein.

[30] M. Bertelli, L. Carlucci, G. Ciani, D.M. Proserpio, A. Sironi, J. Mater. Chem. 7 (1997) 1271 and references therein.
[31] T. Iwamoto, in: J.L. Atwood, J.E.D. Davies, D.D. MacNicol (Eds.), Comprehensive Supramolecular Chemistry, vol. 6, Pergamon, New York, 1996, p. 643.
[32] R.J. Williams, A.C. Larson, D.T. Cromer, Acta Crystallogr. B B28 (1972) 858.
[33] D.T. Cromer, A.C. Larson, Acta Crystallogr. 15 (1962) 397.